Dynamical decoupling with tailored wave plates for long-distance communication using polarization qubits

Bhaskar Roy Bardhan,[1,*] Katherine L. Brown,[1] and Jonathan P. Dowling[1,2]

[1]*Hearne Institute for Theoretical Physics and Department of Physics and Astronomy, Louisiana State University, Baton Rouge, Louisiana 70803, USA*

[2]*Computational Science Research Center, Beijing 100084, China*

(Received 5 February 2013; published 11 November 2013)

We address the issue of dephasing effects in flying polarization qubits propagating through optical fiber by using the method of dynamical decoupling. The control pulses are implemented with half-wave plates suitably placed along the realistic lengths of the single-mode optical fiber. The effects of the finite widths of the wave plates on the polarization rotation are modeled using tailored refractive index profiles inside the wave plates. We show that dynamical decoupling is effective in preserving the input qubit state with the fidelity close to unity when the polarization qubit is subject to the random birefringent noise in the fiber, as well the rotational imperfections (flip-angle errors) due to the finite width of the wave plates.

DOI: 10.1103/PhysRevA.88.052311 PACS number(s): 03.67.Hk, 42.25.Ja, 03.67.Pp, 42.50.Ex

I. INTRODUCTION

Quantum-information processing (QIP) has gained huge interest over the last few decades. This is because it is potentially able to solve many problems faster than the classical counterpart as well as provide secure communication channel. However, the inevitable interaction of the qubits with a noisy environment causes the loss of coherence leading to errors in the processing of the quantum information. This effect is known as decoherence and it limits the time scale over which quantum information can be retained and the distance over which it can be transmitted.

Among the various strategies developed to combat the decoherence effects, we consider the method called dynamical decoupling (DD) [1–8]. This is a relatively simple but effective technique, which uses sequences of external control pulses applied to the system qubits to reduce (or average out) the interaction of the system with the environment. A significant advantage of DD techniques is that they do not require any ancilla qubits or encoding or measurement overheads.

Most of the theoretical works on DD have hitherto considered only the case of ideal pulses. This means that the pulses were assumed to be instantaneous and infinitely strong in the sense of a δ-shaped pulse. In that case, we can ignore the effect of the noise-inducing environment during the application of the pulses. However, in any realistic physical implementation, this is no longer the case as the pulses generally have a finite duration (τ_p). The effects of the applied pulses can be viewed as rotations of the Bloch vector on the unit sphere, and the physical pulses result in rotational imperfections on the Bloch sphere. Such imperfections typically have a cumulative effect, giving rise to accumulation of phase errors in the echo signal. Such an effect leads to considerable reduction in the performance of the DD sequences.

Here, we extend the idea of dynamical decoupling with realistic pulses to long-distance communication using single photons. In optical quantum-information processing, information is usually encoded in the polarization state of photons (which is called a polarization qubit) and photons are then typically routed through optical fibers or waveguides. Transmission of the photons through such optical fibers can be helpful in using them as optical quantum memory [9,10], in distributed quantum computation [11], and in quantum cryptography [12]. For the last few decades, quantum communication using propagation of the single photons through optical fibers has therefore emerged as a very active area of research and commercial development. The initial state of a polarization qubit can usually be very well prepared, while it is much more challenging to preserve this state along the communication channel before it reaches the final detection stage.

As the single photon propagates through the fiber, external effects such as temperature, stress, etc., within the fiber randomly affect the polarization state of the photons [13]. This type of noise is referred to as birefringent noise because these uncontrollable fluctuating factors cause the birefringence, i.e., the refractive index difference $\Delta n = |n_H - n_V|$ (where n_H and n_V denote the refractive indices corresponding to the horizontal and vertical polarizations, respectively) along the fiber to change randomly. The effect results in the polarization state of the single photons to change very rapidly, making it impractical to correct for it by calibration. In practice, optical fibers used for communications with light can be several hundreds of kilometers long and the birefringence in such long optical fibers can totally destroy the information stored in the polarization qubits.

It is therefore crucial to protect the flying polarization qubits against such detrimental dephasing effects induced by the fiber. Several recent studies have looked at suppression of these effects on the polarization qubits. Wu and Lidar [14] showed that dynamical decoupling could be applied for reducing quantum noise in optical fiber. Massar and Popescu presented a method to reduce polarization mode dispersion in optical fibers using controlled polarization rotations [15]. In our previous work [16], we numerically simulated random birefringent noise along realistic fiber length and showed that application of DD could well preserve the input polarization qubit from such noise. We chose the CPMG sequence [17] of DD because this sequence has been shown to be robust against a variety of dephasing and control pulse errors [18–20].

*broyba1@lsu.edu

We restricted our analysis to ideal pulses implemented with zero-width half-wave plates along the fiber.

In this paper, we investigate in detail the issue of polarization dephasing by using *finite-width* wave plates which are likely to cause some additional errors, apart from the random birefringent dephasing noise. Finite widths of the birefringent wave plates directly affect the phase of the photon transmitted through the wave plates leading to further loss of coherence. Introducing tailored refractive index profiles within the wave plates, we show that it is possible to address such detrimental effects with DD techniques when implemented with wave plates at the prescribed locations along the fiber. Estimates of the required inter-wave-plate distance are provided for each of the refractive index profiles, and this information will be enough for an experimenter to know for successfully implementing the faithful long-distance quantum communication channel in practice.

This paper is organized as follows. In Sec. II, we briefly introduce the basic ideas of DD (with ideal and realistic pulses). We discuss the nature of birefringent noise in optical fiber and how the DD techniques can be applied to mitigate such noise with finite-width wave plates in Sec. III. Section IV contains our numerical results and comparative analysis for various tailored refractive index profiles. Finally, we conclude with a brief summary of the results with accompanying discussions.

II. DYNAMICAL DECOUPLING

A. General idea

Dynamical decoupling is an effective method to time-reverse the system-bath interaction by applying sequences of sufficiently fast and strong pulses. As a result of application of the pulse sequence, the interaction of a qubit system with the environment is reduced, thus retaining the quantum information for longer time (or distance). The most general Hamiltonian describing the evolution of a system coupled to a bath can be written as

$$H_{\rm tot} = H_{\rm S} \otimes I_{\rm B} + I_{\rm S} \otimes H_{\rm B} + H_{\rm I}, \tag{2.1}$$

where H_S and H_B are the system and bath Hamiltonians, respectively. Since it is difficult to control the states of the environment, the control pulses need to act on the system, and the effect of these pulses are described as a refocusing of the system-environment interaction by a control Hamiltonian $H_C(t)$. When the system is a qubit undergoing dephasing, we can write the interaction Hamiltonian $H_{\rm I}$ as

$$H_{\rm I} = \sigma_z \otimes B_Z, \tag{2.2}$$

where σ_z is the Pauli Z spin operator and B_Z is a bath operator which couples to the photonic qubit, causing dephasing.

Let us now consider a single cycle of a DD sequence having a period T. The evolution operator describing the evolution of the system from 0 to T (Fig. 1), in the rotating frame, can be written as [21]

$$U(T) = U_f(\tau_{N+1}) \prod_{i=1}^{N} U_C^i(\tau_p) U_f(\tau_i), \tag{2.3}$$

where the free evolution operator in Eq. (2.3) is given by

$$U_f(\tau) = \exp[-i H_{\rm tot}(\tau)], \tag{2.4}$$

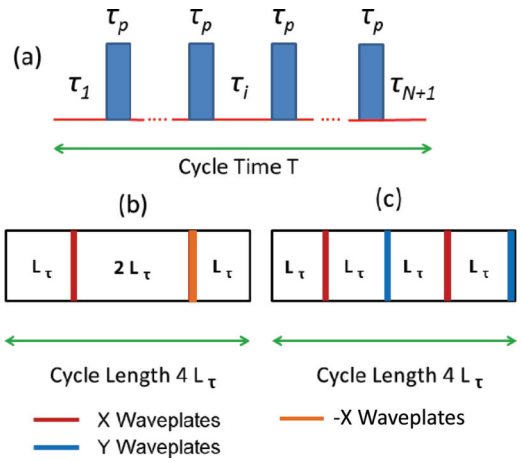

FIG. 1. (Color online) (a) Schematic representation of a cycle of general dynamical sequence with pulses of duration τ_p, (b) CPMG sequence with two pulses in a cycle, and (c) XY-4 sequence with alternated X and Y wave plates. Here X, -X, and Y wave plates implement the π rotations around x, $-x$, and y axes, respectively.

and the evolution operator acting during the application of pulses is

$$U_C^i(\tau_p) = \mathcal{T} \exp\left[-i \int_0^{\tau_p} dt' \left[H_{\rm tot}(\tau) + H_C^i(t')\right]\right]. \tag{2.5}$$

Here $\mathcal{T}$ is the standard time-ordering operator, and the Hamiltonian of the control pulse can be written as

$$H_C(t) = \vec{\sigma} \cdot \vec{f}(t), \tag{2.6}$$

where $\vec{f}(t) = (f_x(t), f_y(t), f_z(t))$ is the vector defining the shape of the pulse and $\vec{\sigma}$ is the vector of the Pauli matrices. The axis of rotation due to the applied pulse at the instant t is given by the unit vector $\frac{\vec{f}(t)}{|\vec{f}(t)|}$ which implies that rotation due to the pulse can be adjusted by tuning the pulse shapes. The underlying principle of dynamical decoupling is to select a "pulse sequence" $f(t)$ which causes the integrated time evolution of the interaction Hamiltonian to coherently average to zero.

Since the evolution described in Eq. (2.3) is necessarily a unitary one, it can be written as the exponential of a Hermitian operator $H_{\rm eff}$

$$U(T) = \exp[-i H_{\rm eff} T], \tag{2.7}$$

where $H_{\rm eff}$ can be written as a series expansion using the average Hamiltonian theory [22]

$$H_{\rm eff} = H^{(0)} + H^{(1)} + \cdots = \sum_{n=0}^{\infty} H^{(n)}. \tag{2.8}$$

An ideal DD sequence, i.e., a DD sequence with instantaneous pulses, makes $H_{\rm eff} = H^{(0)} = H_{\rm B}$ by suppressing the system-bath interaction $H_{\rm I}$, and better performance of a DD sequence usually corresponds to progressively eliminating the higher order terms in such an expansion [2,23,24] (e.g., the Magnus expansion [25]). Prominent examples of DD schemes are the periodic DD (PDD) [4], Carr-Purcell DD (CP) [26], Carr-Purcell-Meiboom-Gill (CPMG) [17], concatenated DD (CDD) [2], and Uhrig DD (UDD) [3].

B. Ideal and real pulses

Ideally, DD pulses are assumed to be strong, instantaneous pulses applied fast enough compared to the internal dynamics of the environment. Under the assumption of weak coupling to the environment, the evolution operator in Eq. (2.5) (in the rotating frame) simplifies to

$$U_C^i(\tau_p) = \exp[-i\sigma_\alpha\theta_p/2]. \tag{2.9}$$

Here $\alpha = x,y,z$ and $\theta_p = \omega_p\tau_p$ (ω_p being the frequency of the pulses) is the rotation around the α axis. For ideal instantaneous pulses which implement π rotations, the angle θ_p will be π.

However, imperfect pulses can result in errors in the rotation axis as well as angle of rotation. We can write the resulting propagator as the product of the ideal pulse propagator and a rotational error $\exp[-i\sigma_{e_i}\theta_{e_i}/2]$ [21], due to the ith wave plate,

$$U_C^i(\tau_p) = \exp\left[-i\sigma_{e_i}\theta_{e_i}/2\right]\exp[-i\sigma_\alpha\theta_p/2]. \tag{2.10}$$

The modified free evolution operator in the presence of the pulse errors can be written as

$$U_f(\tau_i,\tau_p) = U_f(\tau_i)\exp\left[-i\sigma_{e_i}\theta_{e_i}/2\right]. \tag{2.11}$$

The total evolution operation from Eq. (2.3) then reads

$$U(T) = U'_{f_{N+1}}(\tau_{N+1},\tau_p)\prod_{i=1}^{N} U_C^i(0)U'_f(\tau_i,\tau_p). \tag{2.12}$$

The evolution operator in the above expression can then be written as a series expansion similar to Eq. (2.8), and a good choice of DD sequence should make $U(T) \approx \exp(-iH_BT)\mathbb{I}$ (where $\mathbb{I}$ is the identity) in the presence of the pulse errors defined above. Note that the initial system is then preserved against decoherence along with the rotational imperfections, since the factor $\exp(-iH_BT)$ merely acts as a background noise that does not get coupled with the system.

Khodjasteh and Lidar analyzed the cumulative effects in pulse sequences and provided an optimum pulse interval for realistic pulses with a fixed minimal pulse width $\tau_{p,\min}$ [27]. Uhrig and Pasini showed the optimized performance of the DD sequences for considering realistic control pulses of finite duration and amplitude [28,29]. Composite pulse sequences such as BB1, CORPSE, and SCORPSE have been shown to correct systematic pulse errors (which might include pulse amplitude, phase, and frequency errors) [30–34]. Pulse shaping is another method that is used to counteract environmental noise effects during the finite duration of the real pulses [33,35–37].

III. SUPPRESSING BIREFRINGENT DEPHASING WITH DD

A. Effect of birefringent dephasing on the polarization qubits

In a long-distance communication channel (typically of lengths 10–1000 km), often made with polarization-preserving birefringent fiber, polarization qubits are likely to experience random effects due to changes in temperature, stress, etc., during propagation. The characteristic length scales for such changes may be several meters, i.e., lengths smaller than the fiber beat lengths [15,38]. We approximate the communication channel as continuously connected fiber elements which have sections of constant birefringence on the order of this length scale. In the following, we consider the evolution of a pure single-photon state through such a channel.

Assuming that single-photon sources are available, we initialize the qubit in the $+45^\circ$ or -45° state which can be written as

$$|\psi(0)\rangle = \frac{1}{\sqrt{2}}(|H\rangle \pm |V\rangle). \tag{3.1}$$

If we now allow the input photons to propagate through the optical birefringent fiber for a length L, then the phase acquired by the orthogonal polarizations $|H\rangle$ and $|V\rangle$ will be different due to the birefringence. The resulting qubit state can be written as

$$|\psi(L)\rangle = \frac{1}{\sqrt{2}}(e^{i\phi_H}|H\rangle \pm e^{i\phi_V}|V\rangle), \tag{3.2}$$

where the birefringent dephasing $\Delta\phi$ is given by

$$\Delta\phi = \phi_H - \phi_V = (2\pi/\lambda)\int_0^L \Delta n(x)dx. \tag{3.3}$$

Here $\Delta\phi$ is caused by the birefringence $\Delta n(x) = |n_H(x) - n_V(x)|$, which changes along the distance x in the fiber. The off-diagonal density matrix elements (coherence terms) of the polarization state after propagation can be written as

$$\begin{aligned}\rho_{12}(x = L) &= \rho_{12}(0)\langle\exp(-i\Delta\phi)\rangle \\ &\approx \rho_{12}(0)\left(1 - i\langle\Delta\phi\rangle - \frac{\langle\Delta\phi^2\rangle}{2}\right) \\ &= \rho_{12}(0)\exp\left(-\frac{\langle\Delta\phi^2\rangle}{2}\right).\end{aligned} \tag{3.4}$$

In the above equation $\langle\ldots\rangle$ represents the stochastic average, i.e., with respect to the realizations of the birefringent noise. The second line in the above equation follows by expanding the exponential in the first line in series expansion up to the second order of the dephasing $\Delta\phi$. Considering $\Delta\phi$ to be a zero-mean Gaussian process, i.e., $\langle\Delta\phi\rangle = 0$, we obtain the last line in Eq. (3.4) showing that the off-diagonal terms decay exponentially leading to the loss of coherence of the qubit. As a result, the phase of the qubit becomes randomized and the quantum information stored in it is eventually lost.

If we describe the fluctuations in the fiber to be random, then stochastic fluctuations of the refractive index difference $\Delta n(x)$ can be simulated as a Gaussian-distributed zero-mean random process. In this case, the noise is completely defined by the first-order correlation function at two points x_1 and x_2 inside the fiber given by

$$\langle\Delta n(x_1)\Delta n(x_2)\rangle = \exp\left[-\Delta n(x)^2/2\sigma_{\Delta n}^2\right]. \tag{3.5}$$

The above form of the two-point correlation function $\langle\Delta n(x_1)\Delta n(x_2)\rangle$ follows from the fact that the fluctuating random birefringence noise $\Delta n(x)$ is assumed to have Gaussian statistics with $\langle\Delta n\rangle = 0$ and standard deviation $\sigma_{\Delta n}$, leading to the random dephasing $\Delta\phi$ in Eq. (3.3). The separation $|x_1 - x_2|$ between the two points x_1 and x_2 in Eq. (3.5) is considered to be less than correlation length. (Estimates of the correlation lengths for a typical optical fiber are given in Ref. [38].)

B. Choice of DD to preserve the polarization qubit

The facts that the DD pulses are implemented with wave plates in our scheme and that the axis of rotation is fixed by the orientation of the optical axis of the birefringent wave plates highly restrict our choice of DD methods. It is a technically formidable task to have precise control of the varied orientations of the optic axes as required in each sequence of the composite pulse sequences such as BB1, CORPSE, SCORPSE, or KDD (although all of them generally provide robust performance against pulse errors). Moreover, these sequences typically require a large number of pulses in each cycle, which in our case of long-distance fibers affects scalability.

In our case, we have to choose DD sequences which provide robust performance in the presence of our dephasing model, which has randomly distributed noise with the Gaussian spectral density. An optimized sequence such as UDD is also not a good choice, because UDD works best when the noise has a sharp high-frequency cutoff [20,39–41]). In the case of UDD, with single or multiaxis control, pulse errors generally accumulate with higher orders. A few recent studies also indicate that high-order UDD or concatenated DD sequences in general lose their advantage when the pulse intervals are strongly constrained [28,42].

CPMG and XY-4 sequences. To preserve polarization states in a fiber, the CPMG sequence has been shown to work best in such Gaussian-distributed random birefringent noise [16,20, 43]. Another motivation for using CPMG is that this sequence is extremely robust against all pulse imperfections when used with the longitudinal states, while giving marginally better results to preserve the transverse components of polarization [16,18–21,34,44,45]. It requires π rotations around a fixed axis which can be easily set by orienting the optical axis within half-wave plates.

For very similar reasons, we then consider the XY-4 sequence (which requires alternating π rotations around x and y axes), and is known to provide excellent performance in the presence of pulse errors by preserving both the longitudinal and transverse components of polarization [21,34,46,47]. These sequences act as high-pass filters that effectively filter out the components of the $H_{\rm I}$ which vary slowly compared to τ. In both sequences, the total evolution operator after one cycle, defined in Eq. (2.12), is $U_T \approx \mathbb{I} + O(\omega_c^2\tau^2)$ ($\tau_c = 1/\omega_c$ is the correlation time of the environment). Hence, the errors (due to both dephasing and pulse imperfections) resulting in the randomization of the phase of the polarization state coming out of the fiber at the end can be reduced with CPMG and XY-4 up to the first order in $\omega_c\tau$ for each cycle.

IV. NUMERICAL SIMULATIONS AND RESULTS

We focus only on the dephasing noise (i.e., the noise represented by the Pauli Z operator), and neglect the errors due to energy dissipation inside the fiber. This assumption is justified since we restrict our calculations for the wavelengths in the telecommunication band (around 1550 nm) where the optical losses are minimal [48,49].

Simulating birefringent noise. We model birefringent dephasing by continuously concatenating pieces of fiber with randomly generated lengths ΔL. The total propagation length thus can be split into segments of length ΔL with constant birefringence. The phase difference for the ith segment is equal to the sum of $(2\pi/\lambda)\Delta L_i \Delta n_i$. These segments constitute a single phase profile associated with a particular realization of birefringent noise and corresponding changes in the refractive index difference $\Delta n(x)$. Ensemble averaging over profiles gives the density matrix for the output state depicting the random dephasing in the fiber.

The fluctuating random birefringence noise $\Delta n(x)$ in the fiber is simulated as a Gaussian zero mean random process with $\langle \Delta n \rangle = 0$ and standard deviation $\sigma_{\Delta n}$. Since the magnitude of the local birefringence at any point along a birefringent optical fiber is typically of the orders of 10^{-4} to 10^{-7} [50,51], the standard deviation $\sigma_{\Delta n}$ is chosen to have this range of values to mimic the realistic fluctuations in the birefringence.

Implementing DD sequences. We investigate two DD sequences: CPMG and XY-4 applied to the flying polarization qubits propagating through optical fiber. The basic cycles of these two sequences are $f_\tau X f_{2\tau} X f_\tau$ and $f_\tau X f_\tau Y f_\tau X f_\tau Y$, respectively, both with the cycle period of 4τ. The free evolution periods correspond to the phase error accumulated during free propagation along the fiber for a length f_τ, and the X and Y rotations correspond to the π rotations implemented with half-wave plates, as shown in Fig. 1. We make a comparative analysis of these sequences for the following refractive index profiles that are used to generate the errors due to the finite widths of the wave plates.

Generating effects of the finite width. We aim to simulate the effect of finite widths of the wave plates when the polarization qubits are fed into the fiber. In the presence of errors due to such wave plates, from Eq. (2.10) the total propagation operator after one cycle can be written as

$$\begin{aligned} U_C^i(\tau_p) &= \exp\big[-i\sigma_{e_i}\theta_{e_i}/2\big]\exp[-i\sigma_\alpha\theta_p/2] \\ &= \exp[-i(\theta_{p_i} + \Delta\theta_{p_i})\sigma_\alpha]. \end{aligned} \tag{4.1}$$

In our model with finite-width wave plates, the angle error term $\Delta\theta_p$ is the practical deviation from the intended rotation and is due to the refractive index profile $\Delta N(x)$ within the wave plates (which have width Δl). It can be written as

$$\Delta\theta_p = (2\pi/\lambda)\int_0^{\Delta l} \Delta N(x)dx. \tag{4.2}$$

We consider the following refractive index profiles for simulating realistic pulse effects:

$$\Delta N(x) = \begin{cases} \exp\left[-\frac{(x-x_0)^2}{2\sigma^2}\right]; \quad 0 < x_0 < \Delta l & \text{(Gaussian)} \\ 1; \quad 0 < x < \Delta l \text{ and 0 elsewhere} & \text{(rectangular)} \\ \tanh[a(x+1)+1]\tanh[-a(x-1)+1] & \text{(hyperbolic tangent)} \end{cases} \tag{4.3}$$

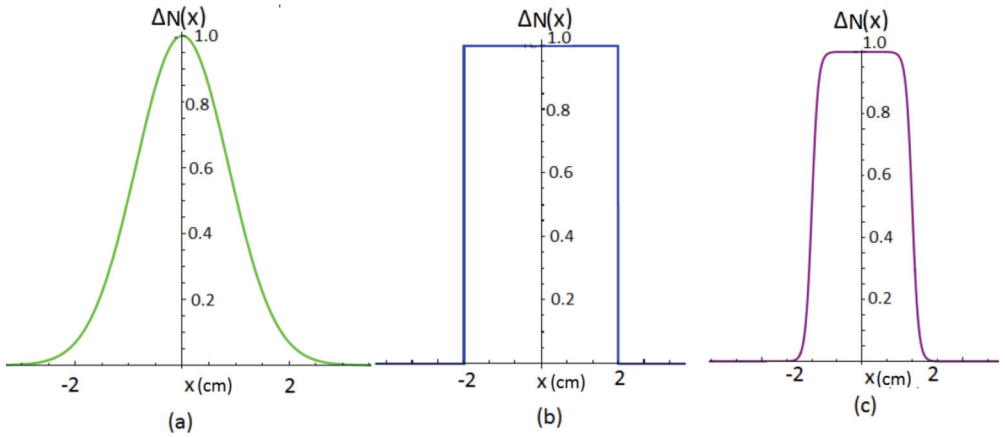

FIG. 2. (Color online) Refractive index profiles $\Delta N(x)$ generating the phase error, where x represents the distance within the wave plate: (a) Gaussian, (b) rectangular, and (c) hyperbolic tangent [as defined in the text and in Eq. (4.2)].

For the Gaussian profile, x_0 and σ denote the mean and the standard deviation of the refractive index distribution within the wave plate, and for the hyperbolic tangent profile the parameter a can be used to adjust the slope of the distribution inside the wave plates. In our simulation, we first consider the flip-angle error of 5%, which is approximately generated by using the parameters $a = 8$, $x_0 = 1$, and $\sigma = 1.8$, from Eqs. (4.2) and (4.3). Refractive index profiles $\Delta N(x)$ for these parameters are shown in Fig. 2.

To characterize the effectiveness of our scheme, we use the fidelity $\mathcal{F}$ between the input state $|\psi_{\rm in}\rangle$ and $\rho_{\rm out}$ as

$$\mathcal{F} = \langle\psi_{\rm in}|\rho_{\rm out}|\psi_{\rm in}\rangle, \tag{4.4}$$

where $\rho_{\rm out} = \frac{1}{n}\sum_{i=1}^{n}|\psi_i\rangle\langle\psi_i|$. Here n is the total number of randomly generated phase profiles, corresponding to the propagation operator $\hat{u}_i$ so that $|\psi_i\rangle = \hat{u}_i|\psi_{\rm in}\rangle$ represents the simulated birefringent noise. Therefore, the fidelity being close to unity implies that the input state is well preserved against the dephasing.

The π rotations required for CPMG and XY-4 sequences are implemented with suitably oriented half-wave plates, and the effects of their finite widths on the relative random phase are generated from the refractive index profiles of Eq. (4.3). In Fig. 3, we show how the fidelity varies and improves with the XY-4 sequence being applied for a realistic fiber length of 10 km, even for a large variation of the parameters of the random dephasing $\Delta\phi$ for the chosen refractive index profiles. Figure 4 illustrates the results for the CPMG sequence for the same length of fiber. In both figures, we considered 5% flip-angle error to make the numerical results comparable.

Fidelity decays without the wave plates (free decays) are also shown in the inset for comparison. In these free decay plots, we note that the fidelity quickly drops to 0.5 even for a small distance (such as 20 m). The reason for this is that the random dephasing in the fiber results in complete phase randomization, and the initial pure state rapidly decays to the fully mixed state (fidelity equal to 0.5 [52,53]). In the main plots of the Figs. 3 and 4, however, the fidelity increases dramatically when the DD sequences are applied with wave plates to suppress the random dephasing in the fiber.

From these figures, we find that while both the sequences work reasonably well to preserve the input polarization states for both the Gaussian and hyperbolic tangent refractive index profiles, the rectangular refractive index profile gives the worst fidelity in both cases. In fact, this profile *never* gives perfect fidelity with the CPMG sequence. In general, the fidelity is preserved better in the XY-4 sequence (Fig. 3) than the CPMG (Fig. 4). This is because the phase errors due to the finite width of the wave plates get partially canceled due to the alternating π rotations around two orthogonal optic axes (x and y) in a XY-4 sequence. It is also interesting to note that the fidelity in general improves with the increasing number of pulses (wave plates) in both cases showing the robustness of these schemes in the sense that the pulse errors tend to cancel each other instead of getting added up.

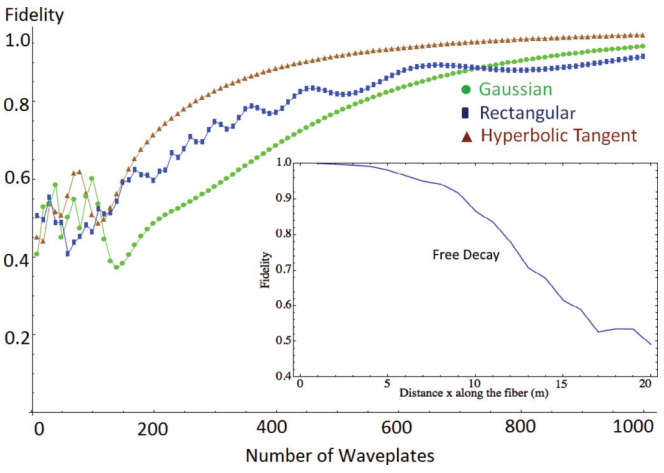

FIG. 3. (Color online) Fidelity obtained with XY-4 wave plates is shown with variation of the number of wave plates for different refractive index profiles. Total length of the optical fiber is 10 km, and number of randomly generated phase profiles to obtain the average fidelity is 500. Inset: Fidelity decay (free decay) without the wave plates in the fiber.

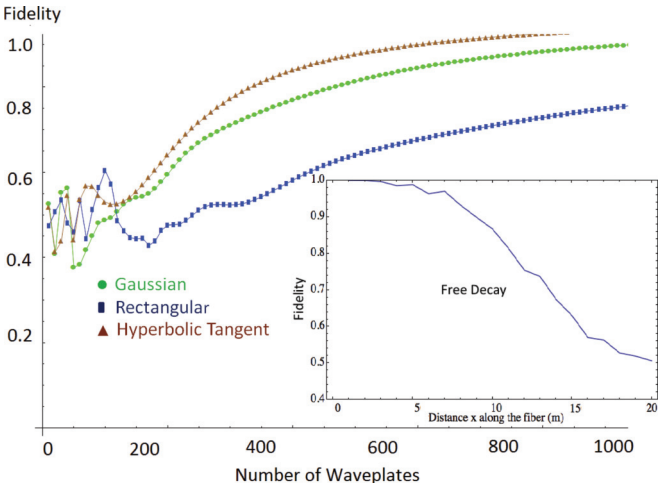

FIG. 4. (Color online) Fidelity obtained with CPMG wave plates shown with variation of the number of wave plates for different refractive index profiles. Total length of the optical fiber is 10 km, and number of randomly generated phase profiles to obtain the average fidelity is 500. Inset: Fidelity decay (free decay) without the wave plates in the fiber.

The required number of wave plates to achieve a given fidelity can also be easily estimated from the above figures. For instance, for the hyperbolic tangent refractive index profiles, the required number of wave plates to achieve a 99.9% fidelity are 840 and 860 for the CPMG and XY-4 sequences, respectively. We also find that fewer wave plates are required for hyperbolic tangent refractive index profiles (for both the sequences) to achieve the same high fidelity, implying that our DD sequences perform best when the finite-width effects are simulated with this particular profile.

Due to the finite widths of the wave plates, the actual angle of rotation deviates from π and this constitutes the flip-angle error in the polarization state of the photon. In Fig. 5, we plot the variations of fidelity with respect to the standard deviation of the birefringent dephasing $\Delta\phi$ and flip-angle errors for both sequences. Here large flip-angle errors up to 50% are considered, and the contour plot shows that the input state is preserved up to fidelity close to unity for a wide variation of the dephasing angle as well as the flip-angle errors.

V. DISCUSSION AND CONCLUSION

For polarization qubits propagating through optical fibers, we demonstrate that the dephasing errors, contributed by both the fiber birefringence and the finite widths of the wave plates, could be suppressed by suitable dynamical decoupling methods. Regardless of the amplitude of the rotational error and random birefringent dephasing, our scheme provides a practical way to tackle them as long as the appropriate wave-plate separations are maintained. As we have dealt with noises due to random fluctuations caused by any possible source such as temperature, stress, etc., the prescribed DD methods can be applied without an experimentalist having a detailed, quantitative knowledge of the decohering environment. To experimentally implement our proposed method to preserve the polarization qubits, several familiar techniques could be suitable depending on the range of fiber lengths one wishes to use. The wave plates may be directly incorporated into the fiber during the manufacturing process. Other methods include writing a Bragg transmission grating periodically into the fiber [54,55], or twisting the fiber in controlled ways causing suitable mechanical stress [13]. Periodic modulations or perturbations in the refractive index in the graded index optical fiber, implementing the desired profiles, can be generated by the techniques described in the Refs. [56–58].

We have successfully shown that it is possible to combat the random birefringent noise in an optical fiber with DD wave plates *which have finite widths*. Our approach provides a practical approach to minimize errors due to both random dephasing noise in the fiber and the rotational errors due to implementation of real finite-width wave plates. This will be helpful in improving the range of quantum communication channels without requiring expensive resources such as ancilla or measurements and hence it leads to immediate commercial

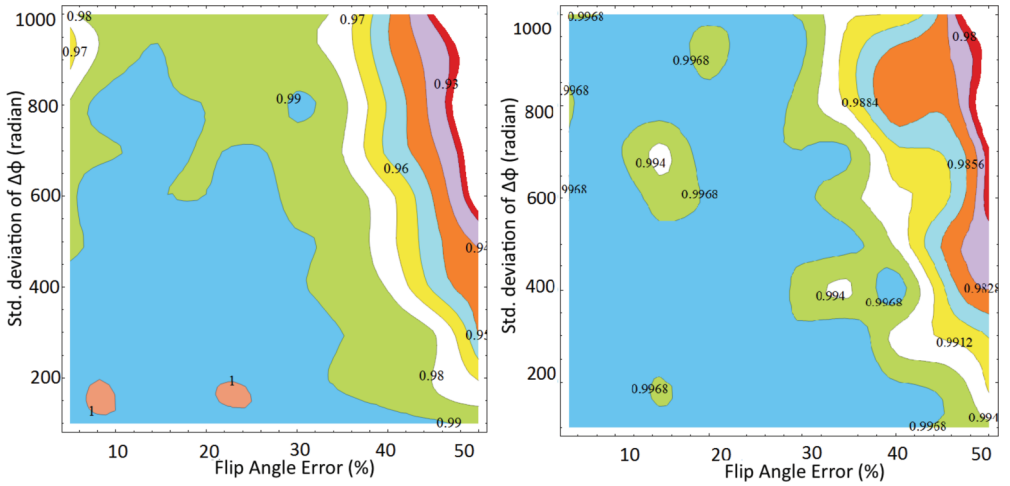

FIG. 5. (Color online) Contour plots of the fidelity with the variations of the standard deviations of the random birefringent dephasing $\Delta\phi$ and the flip angle error for CPMG (left) and XY-4 (right). The simulations are done with fixed number of wave plates (1000) and total length of the fiber $L = 10$ km, and the average fidelity is obtained by taking 500 randomly generated phase profiles.

applications for quantum telecommunication with light. The control overhead in the proposed application of the DD sequences being reasonably small, our scheme will reduce the dephasing error while implementing a scalable quantum computing scheme with photonic qubits.

ACKNOWLEDGMENTS

We gratefully acknowledge the support by the National Science Foundation (NSF) and the Intelligence Advanced Research Projects Activity (IARPA) via Department of Interior National Business Center, Contract No. D12PC00527.

[1] L. Viola and S. Lloyd, Phys. Rev. A **58**, 2733 (1998).
[2] K. Khodjasteh and D. A. Lidar, Phys. Rev. Lett. **95**, 180501 (2005).
[3] G. S. Uhrig, Phys. Rev. Lett. **98**, 100504 (2007).
[4] L. Viola, E. Knill, and S. Lloyd, Phys. Rev. Lett. **82**, 2417 (1999).
[5] L. Viola and E. Knill, Phys. Rev. Lett. **90**, 037901 (2003).
[6] G. S. Uhrig, Phys. Rev. Lett. **102**, 120502 (2009).
[7] J. R. West, B. H. Fong, and D. A. Lidar, Phys. Rev. Lett. **104**, 130501 (2010).
[8] W. J. Kuo and D. A. Lidar, Phys. Rev. A **84**, 042329 (2011).
[9] R. M. Gingrich, P. Kok, H. Lee, F. Vatan, and J. P. Dowling, Phys. Rev Lett. **91**, 217901 (2003).
[10] A. I. Lvovsky, B. C. Sanders, and W. Tittel, Nat. Photon **3**, 706 (2009).
[11] H. J. Kimble, Nature **453**, 1023 (2008).
[12] D. Bouwmeester, A. Ekert, and A. Zeilinger, *The Physics of Quantum Information* (Springer, Berlin, 2000).
[13] R. Ulrich, S. C. Rashleigh, and W. Eickhoff, Opt. Lett. **5**, 273 (1980).
[14] L. A. Wu and D. A. Lidar, Phys. Rev. A **70**, 062310 (2004).
[15] S. Massar and S. Popescu, New J. Phys. **9**, 158 (2007).
[16] B. Roy Bardhan, P. M. Anisimov, M. K. Gupta, K. L. Brown, N. C. Jones, H. Lee, and J. P. Dowling, Phys. Rev. A **85**, 022340 (2012).
[17] S. Meiboom and D. Gill, Rev. Sci. Instrum. **29**, 688 (1958).
[18] R. Freeman, *Spin Choreography: Basic Steps in High Resolution NMR* (Oxford University, London, 1998).
[19] J. J. L. Morton, A. M. Tyryshkin, A. Ardavan, K. Porfyrakis, S. A. Lyon, and G. A. Briggs, Phys. Rev. A **71**, 012332 (2005).
[20] A. Ajoy, G. A. Alvarez, and D. Suter, Phys. Rev. A **83**, 032303 (2011).
[21] G. A. Alvarez, A. Ajoy, X. Peng, and D. Suter, Phys. Rev. A **82**, 042306 (2010).
[22] U. Haeberlen, *High Resolution NMR in Solids: Selective Averaging* (Academic, New York, 1976).
[23] W. Yang, Z. Wang, and R. Liu, Front. Phys. **6**, 2 (2011).
[24] M. J. Biercuk *et al.*, J. Phys. B **44**, 154002 (2011).
[25] S. Blanes *et al.*, Phys. Rep. **470**, 151 (2009).
[26] H. Y. Carr and E. M. Purcell, Phys. Rev. **94**, 630 (1954).
[27] K. Khodjasteh and D. A. Lidar, Phys. Rev. A **75**, 062310 (2007).
[28] S. Pasini and G. S. Uhrig, Phys. Rev. A **81**, 012309 (2010).
[29] G. S. Uhrig and S. Pasini, New J. Phys. **12**, 045001 (2010).
[30] K. R. Brown, A. W. Harrow, and I. L. Chuang, Phys. Rev. A **70**, 052318 (2004).
[31] H. K. Cummins and J. A. Jones, New J. Phys. **2**, 6 (2000).
[32] H. K. Cummins, G. Llewellyn, and J. A. Jones, Phys. Rev. A **67**, 042308 (2003).
[33] M. Mottonen, R. de Sousa, J. Zhang, and K. B. Whaley, Phys. Rev. A **73**, 022332 (2006).
[34] A. M. Souza, G. A. Alvarez, and D. Suter, Phil. Trans. R. Soc. A **370**, 4748 (2012).
[35] S. Pasini, T. Fischer, P. Karbach, and G. S. Uhrig, Phys. Rev. A **77**, 032315 (2008).
[36] L. P. Pryadko and G. Quiroz, Phys. Rev. A **77**, 012330 (2008).
[37] P. Sengupta and L. P. Pryadko, Phys. Rev. Lett. **95**, 037202 (2005).
[38] A. Galtarossa *et al.*, Opt. Lett. **25**, 384 (2000).
[39] M. J. Biercuk *et al.*, Nature **458**, 996 (2009).
[40] E. R. Jenista *et al.*, J. Chem. Phys. **131**, 204510 (2009).
[41] J. Du *et al.*, Nature **461**, 1265 (2009).
[42] G. A. Alvarez, A. M. Souza, and D. Suter, Phys. Rev. A **85**, 052324 (2012).
[43] L. Cywinski, R. M. Lutchyn, C. P. Nave, and S. Das Sarma, Phys. Rev. B **77**, 174509 (2008).
[44] W. M. Witzel and S. Das Sarma, Phys. Rev. Lett. **98**, 077601 (2007).
[45] W. Yao, R. B. Liu, and L. J. Sham, Phys. Rev. Lett. **98**, 077602 (2007).
[46] A. A. Maudsley, J. Mag. Reson. **69**, 488 (1986).
[47] T. Gullion, D. B. Baker, and M. S. Conradi, J. Mag. Reson. **89**, 479 (1990).
[48] P. A. Hiskett *et al.*, New J. Phys. **8**, 193 (2006).
[49] R. H. Hadfield *et al.*, Appl. Phys. Lett. **89**, 241129 (2006).
[50] G. D. VanWiggeren and R. Roy, Appl. Opt. **38**, 3888 (1999).
[51] S. C. Rashleigh *et al.*, Opt. Lett. **7**, 40 (1982).
[52] K. Zyczkowski and H.-J. Sommers, Phys. Rev. A **71**, 032313 (2005).
[53] S. Damodarakurup, M. Lucamarini, G. Di Giuseppe, D. Vitali, and P. Tombesi, Phys. Rev. Lett. **103**, 040502 (2009).
[54] M. Scalora *et al.*, Phys. Rev. E **54**, R1078 (1996).
[55] K. O. Hill and G. Meltz, J. Lightwave Technol. **15**, 1263 (1997).
[56] M. Hisatomi, M. C. Parker, and S. D. Walker, J. Lightwave Technol. **23**, 3551 (2005).
[57] M. Hisatomi, M. C. Parker, and S. D. Walker, J. Lightwave Technol. **23**, 558 (2005).
[58] D. Leduc *et al.*, Meas. Sci. Technol. **18**, 12 (2007).